

Original scientific paper

## Electrochemical sensor for determination of butylated hydroxyanisole in real samples using glassy carbon electrode modified by [Co(HL)<sub>2</sub>Cl<sub>2</sub>] nano-complex

Mahbubeh Fazli and Niloufar Akbarzadeh-T\*

Department of Chemistry, University of Sistan and Baluchestan, P.O. Box 98135-674, Zahedan, Iran

\*Corresponding Author: E-mail: [n.akbarzadeh@chem.usb.ac.ir](mailto:n.akbarzadeh@chem.usb.ac.ir)

Received: February 07, 2023; Revised: February 22, 2023; Published: March 2, 2023

### Abstract

A new mononuclear Co(II) complex with the formula [Co(HL)<sub>2</sub>Cl<sub>2</sub>] (**1**) (HL= N-(2-hydroxy-1-naphthylidene)-2-methyl aniline) has been synthesized and characterized by Fourier transform infrared spectroscopy, UV-Vis, elemental analysis and single crystal X-ray structure analysis. Single crystals of the complex [Co(HL)<sub>2</sub>Cl<sub>2</sub>] (**1**) were obtained through slow evaporation of an acetonitrile solution at room temperature. The crystal structure analysis revealed that the two Schiff base ligands create a tetrahedral geometry via oxygen atoms and two chloride atoms. The nano-size of [Co(HL)<sub>2</sub>Cl<sub>2</sub>] (**2**) have been synthesized by the sonochemical process. Characterization of nanoparticles (**2**) was carried out via X-ray powder diffraction (XRD), scanning electron microscopy (SEM), UV-Vis, and FT-IR spectroscopy. The average sample size synthesized via the sonochemical method was approximately 56 nm. In this work, a simple sensor based on a glassy carbon electrode modified with [Co(HL)<sub>2</sub>Cl<sub>2</sub>] nano-complex was developed ([Co(HL)<sub>2</sub>Cl<sub>2</sub>] nano-complex/GCE) for convenient and fast electrochemical detection of butylated hydroxyanisole (BHA). The modified electrode offers considerably improved voltammetric sensitivity toward BHA compared to the bare electrode. Applying linear differential pulse voltammetry, a good linear relationship of the oxidation peak current with respect to concentrations of BHA across the range of 0.5–150 μM and a detection limit of 0.12 μM was achieved. The [Co(HL)<sub>2</sub>Cl<sub>2</sub>] nano-complex/GCE sensor was applied to the determination of BHA in real samples successfully.

©2023 by the authors. This article is an open-access article distributed under the terms and conditions of the Creative Commons Attribution license (<http://creativecommons.org/licenses/by/4.0/>).

### Keywords

Schiff base ligand; cobalt(II) nano-complex; butylated hydroxyanisole; voltammetry

### Introduction

Butylated hydroxyanisole, a substituted phenolic compound, is one of the potent chemical antioxidants used as a preservative in food, food packaging, animal feed, cosmetics, pharmaceutical preparation, rubber and petroleum products. It is also used as a vitamin A stabilizer. BHA is added to food products to improve their stability, especially to prevent rancidity in products containing lipids or fats. BHA is exclusively used in food products because of its ability to remain active even at high temperatures while cooking or baking [1-3]. Although they are powerful in protecting product quality in food distribution, excess antioxidants added to food might produce toxicities or mutagenicities and, thus, endanger people's health [4,5]. Thus, it is necessary to reliably determine the amounts of BHA in food or other products.

Many methods, including spectrophotometry [6], gas chromatography [7], high-performance liquid chromatography [8], micellar electrokinetic capillary chromatography [9] and electrochemical methods [10,11] have been developed for the determination of BHA. Electrochemical sensors with excellent ability for the determination of electroactive substances, especially food samples, have been suggested as a powerful analytical tool in recent years [12-18]. Electrochemical sensors are fast, portable and affordable. However, in many cases, the detection limit was insufficient when traces of these compounds had to be determined. The results might also be irreproducible due to surface fouling, requiring high oxidation potentials and being time-consuming [19-26]. Chemically modified electrodes (CMEs) improve the sensitivity and selectivity of electrochemical analysis by improving the kinetics of the reaction via an electrocatalytic process at the CME surface [24-35].

Recently, more attention has been focused on the synthesis and application of nanoparticles (NPs), and on properties of NPs such as high electrical conductivity, high surface area, and chemical stability [36-40]. The NPs can be used to promote electron transfer reactions when it is used as electrode material in an electrochemical device. Therefore, the modification of the electrochemical interface by nanostructures is one of the recent approaches used extensively in the development of sensing platforms [41,43].

Schiff base ligands are among the most common coordinating ligands in coordination chemistry [44], through a direct forward condensation reaction between an amine and a carbonyl compound [45]. During the past few decades, considerable attention has been paid to the chemistry of metal complexes of Schiff bases containing nitrogen and other donor atoms [46]. This may be attributed to their stability, biological activity and potential applications in many fields, such as oxidation catalysis, electrochemistry [47], and biological properties, such as antibacterial, antifungal and antioxidant activities [48,49]. In general, the antibacterial and antifungal activities of Schiff bases are attributed to the presence of lone pair of electrons on the nitrogen atom and the electron-donating character of the double bond of the azomethine group [50]. Facile and inexpensive synthesis, allied with the wide range of structural and electronic features of Schiff bases and their coordination complexes, has increased interest in chemically modifying electrodes with these compounds. Therefore, the resulting electrodes have been used as sensors and/or probes in a variety of fields. All this interest has culminated in the development of low-cost sensors. In particular, the many structural and electronic properties of Schiff bases and their transition metal nano-complexes allow them and the analyte to establish different interactions, which improves sensor selectivity and sensitivity [51-56].

In this work, Schiff base ligand [HL] and its cobalt(II) complex (**1**) with (N-(2-hydroxynaphtalen)2-methyl aniline) Schiff base ligand were synthesized. The complex was characterized using spectroscopic techniques such as FT-IR, UV-Vis and elemental analysis. The crystal structure of title complex was determined by X-ray crystallography. The Schiff base cobalt nano-complex (**2**) was prepared by the sonochemical method. This synthesis was performed without the use of any surfactants. The nano-sized complex (**2**) was identified using XRD and SEM techniques. Also, we developed a voltammetric sensor based on  $[\text{Co}(\text{HL})_2\text{Cl}_2]$  nano-complex modified glassy carbon electrode for the detection of BHA. Under optimal conditions, the sensor displayed excellent sensitivity, low detection limit and rapid response toward the analyte. Moreover, this developed sensor was applied in the determination of BHA in real samples successfully

## Experimental

### *Materials and instrumentation*

$^1\text{H-NMR}$  spectrum was accomplished with Bruker AVANCE3 3-300MHz spectrometer using DMSO- $d_6$  as solvent and at room temperature (298 K). Fourier-transform infrared spectra were performed on a PerkinElmer FT-IR spectrophotometer model spectrum two with KBr discs in the range of 4000-400  $\text{cm}^{-1}$ . For

elemental analyses of new compounds, a Costech ECS 4010 CHNS Elemental Analyzer was utilized. UV-Vis spectra were recorded in the range of 200–800 nm on Optizen view 2120UVplus Spectrophotometer ver1-2. Single crystal measurements were done with Rigaku OD Supernova, equipped with Atlas S2 CCD detector and Mo-K $\alpha$  radiation from a micro-focused sealed X-ray tube. The data reduction, scaling and absorption correction were made in CrysAlis PRO. MCE was used for the visualization of electron density maps.

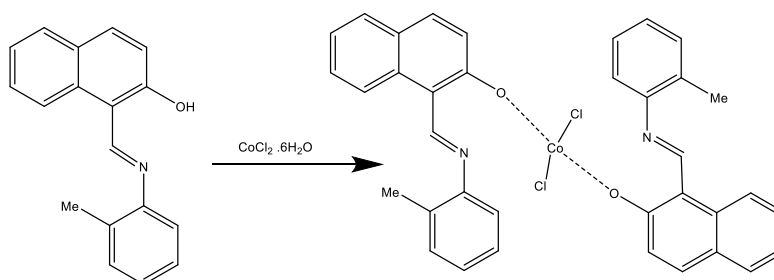
All the electrochemical measurements were carried out on a PGSTAT302N potentiostat/galvanostat Autolab consisting of a traditional three-electrode system: a bare or modified glassy carbon electrode (GCE) as the working electrode, an Ag/AgCl as the auxiliary electrode and a Pt wire as the counter electrode. Solution pH values were determined using a 713 pH meter combined with a glass electrode (Metrohm, Switzerland). BHA and other chemicals used were analytical grade and were purchased from Sigma Aldrich and Merck. Orthophosphoric acid was used to prepare the phosphate buffer solutions (PBSs), and sodium hydroxide was used to adjust the desired pH values (pH range between 2.0 and 9.0).

#### Synthesis of Schiff base ligand [HL]

The ligand (HL: N-(2-hydroxy-1-naphthylidene)-2-methyl aniline) was synthesized by adding a solution of 2-hydroxy-1-naphthaldehyde (0.17 g, 1 mmol) in 10 mL of ethanol to a solution of 2-methyl aniline (0.11 ml, 1 mmol). Then, the mixture was refluxed for 6 h. The resulting yellow solution was placed at room temperature. After 24 h, yellow crystals of [HL] were formed. The Schiff base ligand was characterized by  $^1\text{H-NMR}$ , FT-IR, elemental analysis and single-crystal X-ray diffraction: mp:(154 °C);(yield: 88 %);(MW: 261.31); Anal. Calc. for  $[\text{C}_{18}\text{H}_{15}\text{NO}]$ : C82.73;H6.12; N 5.79; Found: C82.70; H6.09; N5.76. FTIR (KBr,  $\text{cm}^{-1}$ ), 3421v (N-H), 1620 v(C=N), 1161 v(C-O), 1479 v(C=C);  $^1\text{H-NMR}$  (300 MHz, DMSO  $d_6$ , ppm) 9.61 (1H, s, CH=N), 16.05 (1H, OH), 2.40 (3H,CH $_3$ ) [37].

#### Synthesis of complex (1)

The Schiff base ligand (HL: N-(2-hydroxy-1-naphthylidene)-2-methyl aniline) (0.26 g,1 mmol) was dissolved in 10 ml of methanol and to this yellow solution, a solution of  $[\text{CoCl}_2 \cdot 6\text{H}_2\text{O}]$  (0.12 g, 0.5mmol) in 10 ml of methanol was added dropwise. The reaction mixture was refluxed for 6 h. The complex was precipitated, and the precipitate was filtered and dried at room temperature. Green crystals of  $[\text{Co}(\text{HL})_2\text{Cl}_2]$  complex suitable for single crystal X-ray diffraction were obtained by the crystallization from the acetonitrile solution of the precipitate after two weeks. The complex was characterized by UV-Vis, FT- IR, elemental analysis and single-crystal X-ray diffraction (Scheme 1). mp:250 °C; (yield: 85 %); (MW: 652.5); Anal. Calc. for  $[\text{C}_{36}\text{H}_{30}\text{Cl}_2\text{CoN}_2\text{O}_2]$ : C66.27; H4.63; N4.29; found: C66.32; H4.69; N4.27. FT-IR (KBr,  $\text{cm}^{-1}$ ), 1619 v(C=N); 1146 v(C-O), 535 v(Co-O).



**Scheme1.** Synthetic route for complex (1).

#### Synthesis of nanocomplex (2)

A solution of  $\text{CoCl}_2 \cdot 6\text{H}_2\text{O}$  (0.12 g, 0.5 mmol) in methanol (10 mL) was positioned in a high-density ultrasonic probe for 10 min. Then to this solution, 10 ml of methanolic solution of Schiff base ligand (0.26 g, 1 mmol) was added dropwise. The resultant solution was then irradiated for 60 min at 60 °C with a power of 100 W.

The obtained brown precipitate was filtered and dried in air. mp: 245 °C; (yield: 87 %); (MW: 652.5); Anal. Calc. for  $[C_{36}H_{30}CoCl_2N_2O_2]$ : C 66.27; H 4.63; N 4.29; found: C 66.34; H, 4.69; N, 4.27. FT-IR (KBr,  $cm^{-1}$ ): 1621  $\nu(C=N)$ ; 1147  $\nu(C-O)$ , 534  $\nu(Co-O)$ .

#### Preparation of $[Co(HL)_2Cl_2]$ nano-complex/GCE

The bare glassy carbon electrode was coated with  $[Co(HL)_2Cl_2]$  nano-complex according to the following simple procedure. 1 mg  $[Co(HL)_2Cl_2]$  nano-complex was dispersed in 1 mL aqueous solution within 50 min ultrasonication. Then, 4  $\mu$ l of the prepared suspension was dropped on the surface of carbon working electrodes. It remains at room temperature until it becomes dry. The surface areas of the  $[Co(HL)_2Cl_2]$  nano-complex/GCE and the un-modified GCE were obtained by CV using 1 mM  $K_3Fe(CN)_6$  at various scan rates. Using the Randles–Ševčík equation for  $[Co(HL)_2Cl_2]$  nano-complex/GCE, the electrode surface was found to be 0.109  $cm^2$  which was about 3.5 times greater than un-modified GCE.

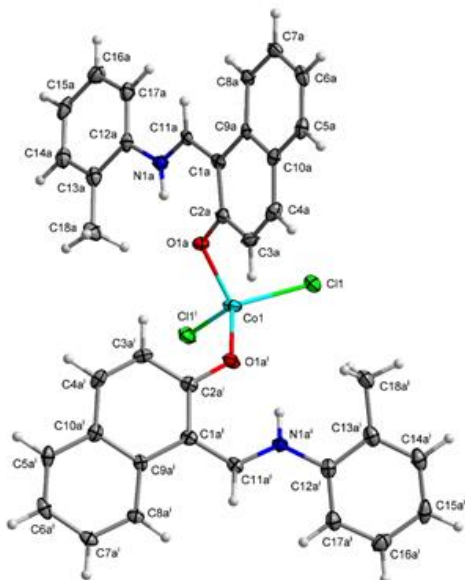
## Results and discussion

### Single crystal X-ray diffraction

Green crystals of  $[Co(HL)_2Cl_2]$  (**1**) were obtained by slow evaporation of an acetonitrile solution. Its structure was determined by single-crystal X-ray diffraction. The complex crystallized in the monoclinic system in space group  $C2/c$  with an asymmetric unit consisting of a metal cation in a special position, one chloride anion and one disordered HL ligand. Table 1 shows the crystallographic data for complex (**1**).

All hydrogen atoms of the strongly occupied part of ligands were discernible in difference Fourier maps and could be refined to reasonable geometry. According to common practice, H atoms bonded to C were kept in ideal positions with  $C-H = 0.96 \text{ \AA}$ , while positions bonded to N were refined with restrained bond length. In both cases,  $U_{iso}(H)$  was set to  $1.2U_{eq}(C, N)$ . All non-hydrogen atoms were refined using harmonic refinement. A disordered ligand was observed in both structures. Given the scale of disorder and numerous overlaps, we decided to use molecular refinement to model the disorders. Two models were used to allow for free rotation of the tolyl group. The occupancies of two positions were refined with the sum constrained to 1. Resulting occupancy ratios were 832(2):168(2). For further information on data collection and refinement, see Table 1.

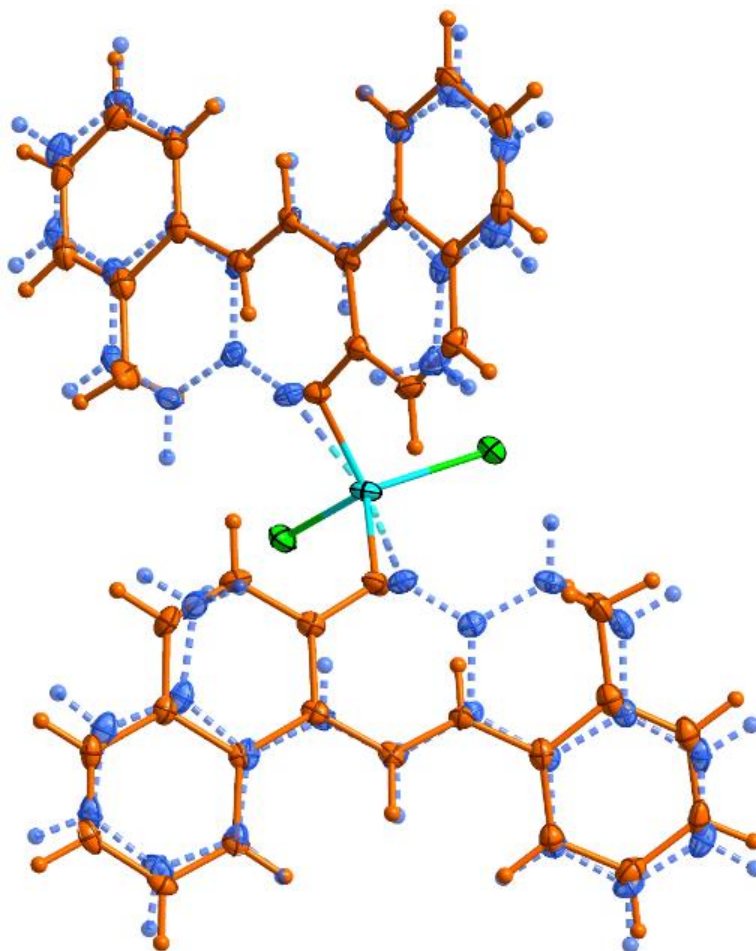
A view of compound (**1**) is shown in Figure 1. The occupied position is shown in Figure 2.



**Figure 1.** The labeled diagram of compound (**1**). Thermal ellipsoids are at 50% probability level symmetry code: (i) 1-x, y, 0.5-z.

**Table 1.** Crystallographic data and refinement parameters for complex (1)

Compound	(1)
Formula	C <sub>36</sub> H <sub>30</sub> Cl <sub>2</sub> CoN <sub>2</sub> O <sub>2</sub>
Formula weight (g mol <sup>-1</sup> )	652.5
λ (Å)	0.71073
crystal system	monoclinic
space group	C 2/c
Hall group	-C 2yc
a (Å)	24.3845(7)
b (Å)	7.5848(3)
c (Å)	17.9596(9)
β (°)	114.763(3)
T (K)	95
V (Å <sup>3</sup> )	3016.2(2)
Z	4
D <sub>calc</sub> (g cm <sup>-3</sup> )	1.437
μ (mm <sup>-1</sup> )	0.784
F(000)	1348
h,k,l <sub>max</sub>	33,10,15
θ <sub>max</sub> (°)	29.34
Measured refl.	7862
Indep. refl. (R <sub>int</sub> )	3594 (0.018)
Obs. refl. (I>3σ(I))	3110
R <sub>1</sub> (obs)	0.0343
wR <sub>2</sub> (all)	0.0998
S	1.510
Parameters	211
Δρ <sub>max</sub> , Δρ <sub>min</sub> (e Å <sup>-3</sup> )	0.35, -0.36
CCDC	1995453

**Figure 2.** Disorder in complex (1), weakly occupied position depicted in blue with dashed bonds.

The cation in complex (1) is four-coordinate with two chloride anions and two phenolic oxygen atoms forming a slightly distorted tetrahedron. Only the oxygen atom of the neutral zwitterionic HL ligand is coordinated with the metal cation, while the presence of an azomethine proton denies the possibility of coordination via the nitrogen atom. A list of the most important bond distances and angles is reported in Table 2.

**Table 2.** Selected bond lengths and angles in structures (1) and (2)

X–Y	(1) X–Y (Å)	X–Y–Z	(1) X–Y–Z (°)
Co–Cl1	2.2505(5)	Cl1–Co–Cl1 <sup>i</sup>	115.11(2)
Co–Cl1 <sup>i</sup>	2.2505(5)	Cl1–Co–O1a	104.82(6)
Co–O1a	1.9618(16)	Cl1–Co–O1a <sup>i</sup>	110.14(5)
Co–O1a <sup>i</sup>	1.9618(16)	Cl1 <sup>i</sup> –Co–O1a	110.14(5)
Co–O1b	2.122(16)	Cl1 <sup>i</sup> –Co–O1a <sup>i</sup>	104.82(6)
Co–O1b <sup>i</sup>	2.122(16)	O1a–Co–O1a <sup>i</sup>	111.97(7)
		Cl1–Co–O1b	114.6(2)
		Cl1–Co–O1b <sup>i</sup>	99.06(19)
		Cl1 <sup>i</sup> –Co–O1b	99.06(19)
		Cl1 <sup>i</sup> –Co–O1b <sup>i</sup>	114.6(2)
		O1b–Co–O1b <sup>i</sup>	115.4(3)

Symmetry code: (i) 1-x, y, 0.5-z.

The coordination tetrahedron formed by chloride anions and the ligand with higher occupancy has only minor distortions from the ideal values with Co–Cl1 bond lengths at 2.2505(5) Å and Co–O1a bond lengths at

1.9618(16) Å. The bond angles are in the range from 104.82(6)° to 115.11(2)°. The coordination of weakly occupied oxygen atoms appears weaker compared to the oxygen atoms with higher occupancy, with Co–O1b bonding longer by 0.1602 Å compared to Co–O1a. This elongation brings the bond length closer to the length of Co–Cl1 bond, which should result in lower distortions from the ideal tetrahedron. Regardless of the similarities in the bond lengths, the distortions in the coordination tetrahedron formed with the weakly occupied ligand were even more pronounced, with the angles ranging from 99.06(19)° to 115.4(3)°.

#### FT-IR spectra

The FT-IR analysis data is listed in Table 3. The FT-IR spectrum of the free Schiff base ligand [HL] exhibits a band in 3421 due to  $\nu(\text{NH}^+)$  and a band in 1620  $\text{cm}^{-1}$  due to  $\nu(\text{C}=\text{N})$  azomethine. A band at 1161  $\text{cm}^{-1}$  is assigned to the  $\nu(\text{C}-\text{O})$  phenolic group. This band has been shifted to lower frequencies for both complex (1) and nano-complex (2), in the region of 1146-1147  $\text{cm}^{-1}$ , which indicates that both compounds are formed by the coordination of the oxygen atom of [HL] to the metal ion (Figure 3). FT-IR spectra of both complex (1) and nanocomplex (2) show weak bands at 535  $\text{cm}^{-1}$  and 534  $\text{cm}^{-1}$  that assign to (Co-O), and don't show any shift due to  $\nu(\text{C}=\text{N})$  and  $\nu(\text{NH}^+)$  that this display the azomethine group of [HL] doesn't participate in complex formation [57].

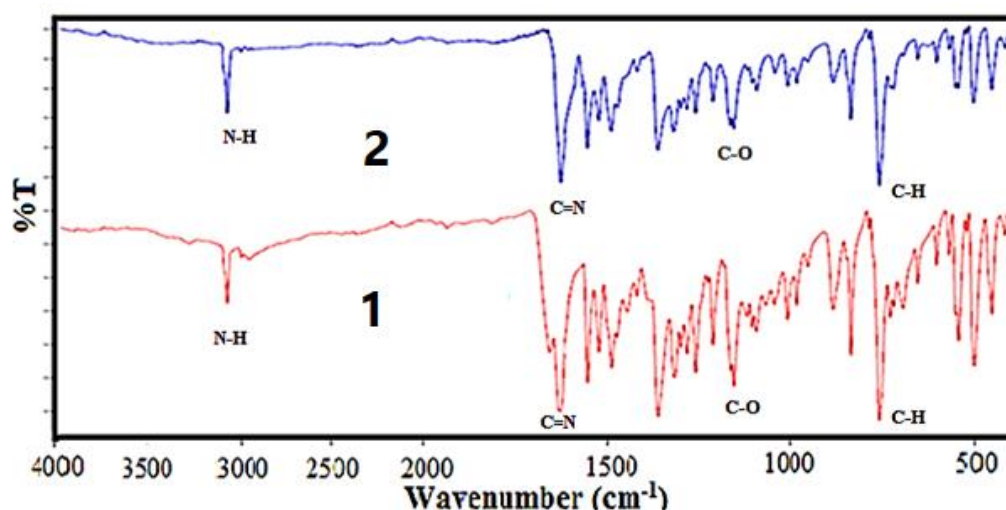


Figure 3. The FT-IR spectra of the complex (1) and its nanoparticles (a2)

Table 3. Selected IR frequencies ( $\text{cm}^{-1}$ ) of [HL], (1) and (2).

compound	$\nu(\text{N-H})$	$\nu(\text{C}=\text{N})$	$\nu(\text{C}-\text{O})$	$\nu(\text{Co}-\text{O})$
HL	3421	1620	1161	-
Co(HL) <sub>2</sub> Cl <sub>2</sub> (1)	3425	1619	1146	535
Co(HL) <sub>2</sub> Cl <sub>2</sub> (2)	3425	1621	1147	534

HL: N-(2-hydroxy-1-naphthylidene)-2-methyl aniline

#### UV-Vis spectra

UV-Vis spectra of [HL], (1) and (2) in methanol solution contain different peaks related to the transition bands data. These absorption bands (nm) are listed in Table 2. The Schiff base ligand display two bands at 230 and 250 nm attributed to  $\pi \rightarrow \pi^*$  and a band at 330 nm that is assigned to  $n \rightarrow \pi^*$  transitions. In the electronic spectra of both (1) and (2), intra-ligand transitions ( $n \rightarrow \pi^*$  and  $\pi \rightarrow \pi^*$ ) were shifted to another wavelength that this is due to the coordination of the metal to the ligands. Both of electronic spectra of complex (1) and nano-complex (2) showed three d-d absorption bands at 520-635 nm are assigned to the transition  ${}^4A_2 \rightarrow {}^4T_2(\text{F})$ ,  ${}^4A_2 \rightarrow {}^4T_1(\text{F})$  and  ${}^4A_2 \rightarrow {}^4T_1(\text{P})$ , respectively [58] (Figures 4 and 5).

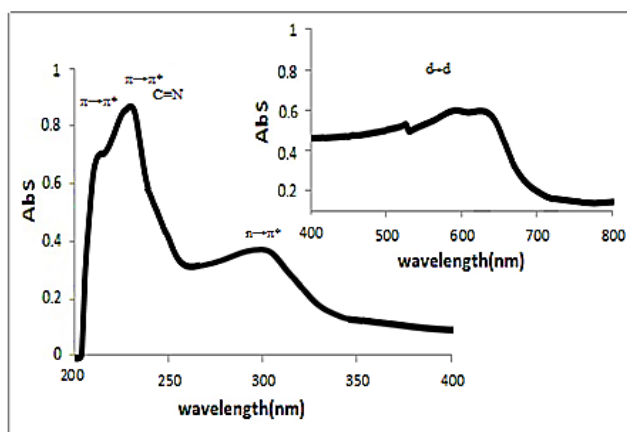


Figure 4. The spectrum of UV-Vis of (1) in methanol.

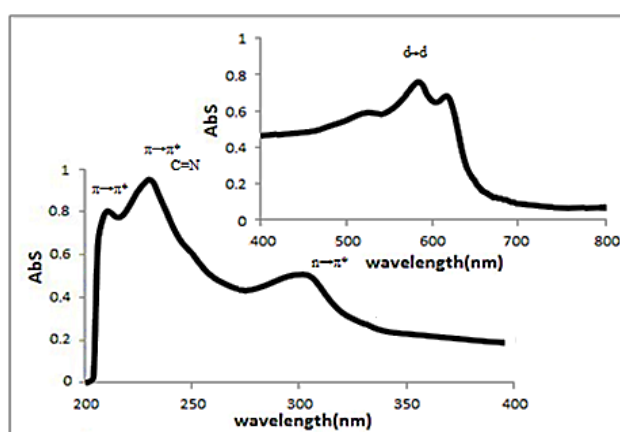


Figure 5. The spectrum of UV-Vis of (2) in methanol.

#### XRD and SEM

The XRD patterns of nano-sized Co(II) complex (2) and standard powder Co(II) complex (1) were obtained from single-crystal X-ray diffraction and are exhibited in Figure 6. The XRD pattern shows the crystalline phase and the nature of the complex. By investigating the location and intensity of the peaks of both patterns, it can be deduced that the diffraction angle in both complexes obtained by different methods is the same [59]. This indicates that the nano-sized complex (2) has a single crystalline phase that this phase is similar to that obtained by single-crystal X-ray diffraction [60]. The width of the diffraction peaks shows the nanocrystal complex (2) particles are of nanometer scales [61]. The particle means the size of the nanocrystal complex (2) was calculated using the Debye Scherrer equation. SEM images of the nanocrystal complex (2) are shown in Figure 7. The SEM photos also show the shape of the nanoparticles and the surface morphology of the nanocrystal complex. The average size diameter obtained from the Debye-Scherrer equation of nanocrystal complex (2) was approximately 56 nm.

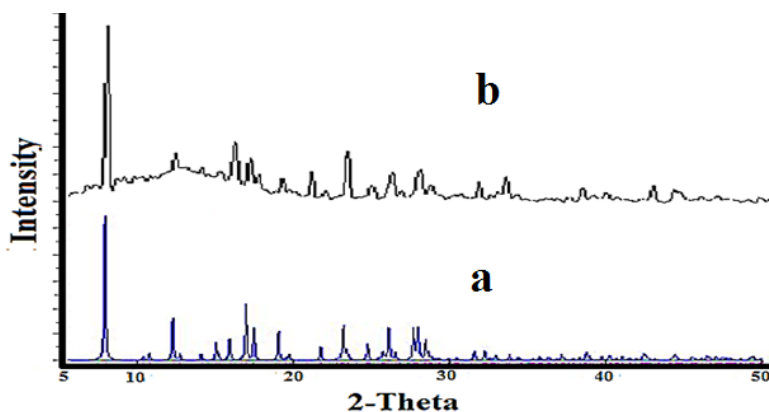


Figure 6. The XRD patterns of a: standard powder Co(II) complex (1) b: nano-sized Co(II) complex (2)

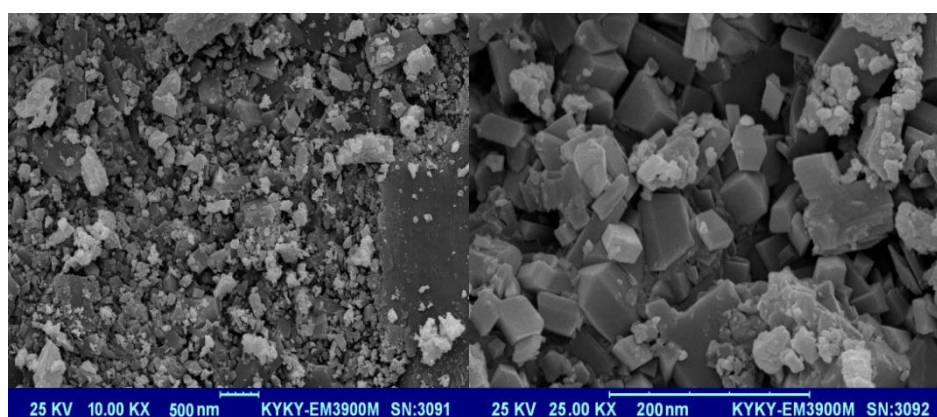
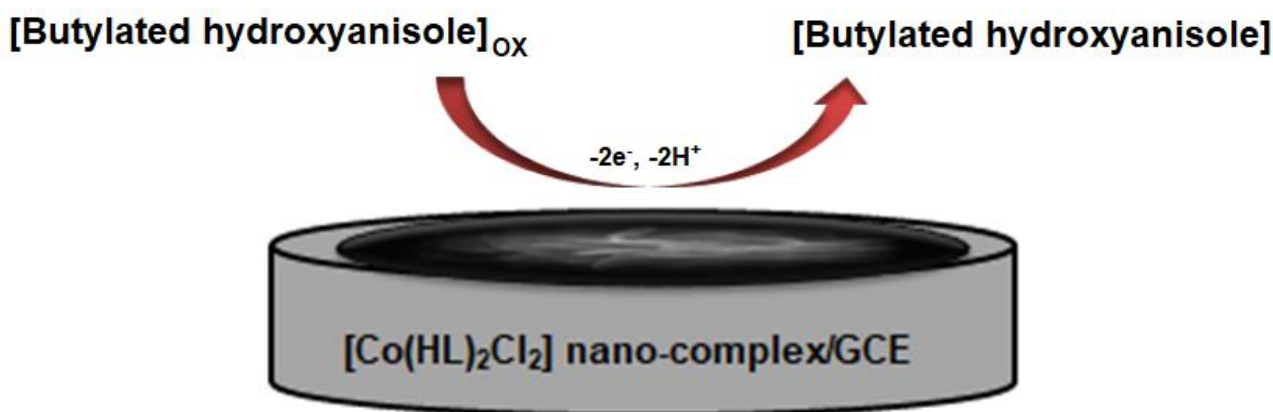


Figure 7. SEM images of the nanocrystal complex (2)

*Electrochemical behavior of BHA at the surface of various electrodes*

According to our knowledge, the electrooxidation of BHA is closely related to the pH value of the solution (Scheme 2). So, the effect of pH was investigated using the differential pulse voltammetry (DPV) method. The results show that the oxidation peak current increased from pH 2.0 to 7.0, and then the current conversely decreased when the pH value increased from 7.0 to 9.0. According to obtained results, pH 7.0 was chosen as the best optimal experimental condition for other experiments.



**Scheme 2.** The proposed mechanism for the oxidation of BHA at the  $[\text{Co}(\text{HL})_2\text{Cl}_2]$  nano-complex/GCE.

The electrochemical behavior of BHA was investigated by linear sweep voltammetry (LSV). The linear sweep voltammograms obtained using the bare GCE and  $[\text{Co}(\text{HL})_2\text{Cl}_2]$  nano-complex/GCE in 0.1 M PBS (pH 7.0) in the presence of 50.0  $\mu\text{M}$  BHA are shown in Figure 8. At the bare CPE, a weak oxidation peak current ( $i_{\text{pa}} = 3.6 \mu\text{A}$ ) could be seen at 0.57 V. In contrast,  $[\text{Co}(\text{HL})_2\text{Cl}_2]$  nano-complex/GCE exhibited an enhanced sharp anodic peak current ( $i_{\text{pa}} = 9.4 \mu\text{A}$ ) at much lower overpotential  $E_p = 0.43$  V. These results confirmed that the  $[\text{Co}(\text{HL})_2\text{Cl}_2]$  nano-complex improved the sensitivity of the modified electrode by enhancing peak current and decreasing the overpotential of the oxidation of BHA.

*Effect of scan rate on the determination of BHA at  $[\text{Co}(\text{HL})_2\text{Cl}_2]$  nano-complex/GCE*

The influence of the scan rate ( $\nu$ ) on the peak currents ( $i_{\text{pa}}$ ) of BHA at  $[\text{Co}(\text{HL})_2\text{Cl}_2]$  nano-complex/GCE was investigated by LSV. Figure 9 shows the voltammetric response of 50.0  $\mu\text{M}$  BHA at  $[\text{Co}(\text{HL})_2\text{Cl}_2]$  nano-complex/GCE at different scan rates in the range of 10 to 400 mV/s. The oxidation peak current of BHA increases linearly with increasing scan rate. A linear regression equation was obtained from the plot  $i_{\text{pa}}$  and  $\nu^{1/2}$  (square root of scan rate) as follows;  $i_{\text{pa}} (\mu\text{A}) = 1.3684 \nu^{1/2} (\text{mV/s})^2 - 0.5184$  ( $R^2 = 0.9995$ ) for the oxidation process, which indicates that the reaction of BHA at  $[\text{Co}(\text{HL})_2\text{Cl}_2]$  nano-complex/GCE is diffusion controlled.

In order to obtain some information on the rate-determining step, we drew a Tafel plot (Figure 10) using the data from the rising part of the current-voltage curve recorded at a low scan rate of 10  $\text{mV s}^{-1}$  for 50.0  $\mu\text{M}$  BHA. The linearity of the  $E$  versus  $\log I$  plot implies the intervention of the kinetics of the electrode process. The slope of this plot can be used to estimate the number of electrons transferred in the rate-determining step. According to Figure 10 inset, the Tafel slope for the linear part of the plot was estimated to be equal to 0.1316 V. The value of the Tafel slope indicates that the one-electron transfer process is the rate-limiting step, assuming a transfer coefficient ( $\alpha$ ) of about 0.55.

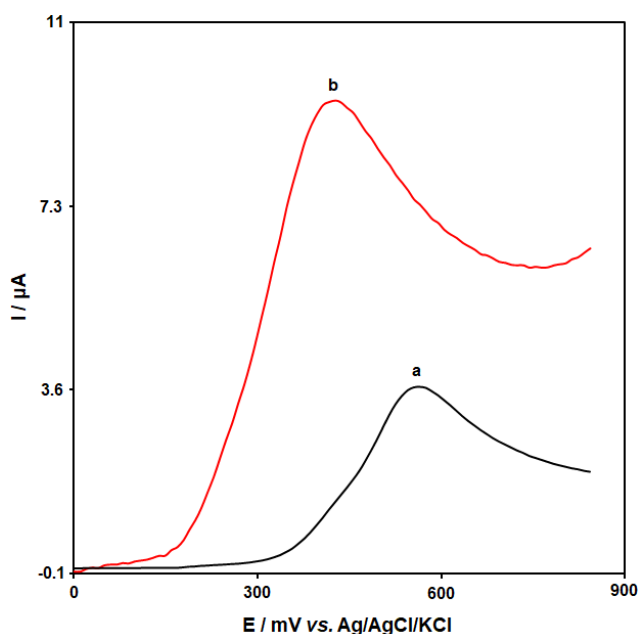


**Figure 8.** The linear sweep voltammograms of (a) bare GCE and (b) [Co(HL)<sub>2</sub>Cl<sub>2</sub>] nano-complex/GCE in 0.1 M PBS (pH 7.0) in the presence of 50.0 μM BHA at the scan rate 50 mVs<sup>-1</sup>.

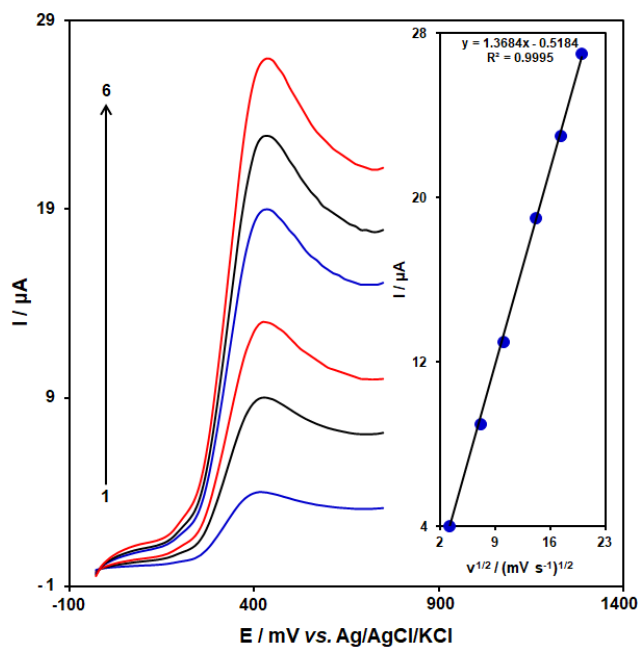


**Figure 9.** Linear sweep voltammograms of [Co(HL)<sub>2</sub>Cl<sub>2</sub>] nano-complex/GCE in 0.1 M PBS (pH 7.0) containing 50.0 μM BHA at various scan rates; 1-6 correspond to 10, 50, 100, 200, 300, and 400 mV s<sup>-1</sup>, respectively. Inset: variation of anodic peak current vs.  $v^{1/2}$ .

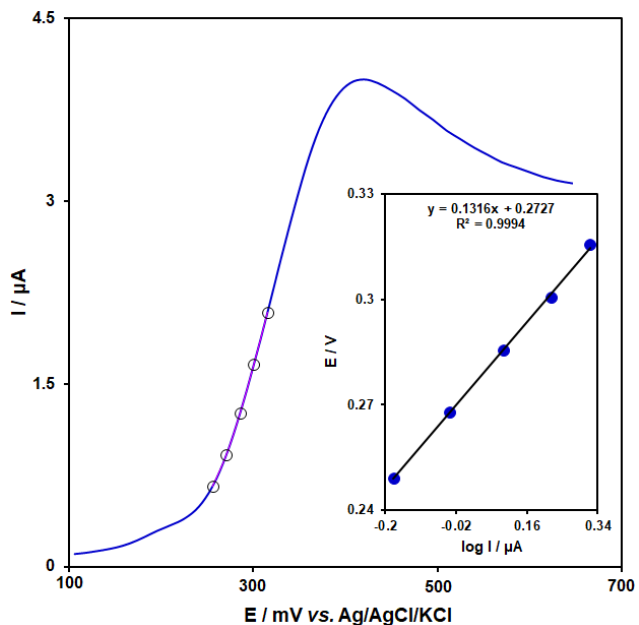


**Figure 10.** Linear sweep voltammograms response for 50.0 μM BHA with 10 mVs<sup>-1</sup> scan rate. Inset: The Tafel plot derived from the rising part of the corresponding voltammogram.

### Chronoamperometric analysis

The analysis of chronoamperometry for BHA samples was performed by use of  $[\text{Co}(\text{HL})_2\text{Cl}_2]$  nano-complex/GCE vs. Ag/AgCl/KCl (3.0 M) at 0.48 V. The chronoamperometric results of different concentrations of BHA in PBS (pH 7.0) are demonstrated in Figure 11. The Cottrell equation for the chronoamperometric analysis of electroactive moieties under mass transfer limited conditions is as follow:

$$I = nFAD^{1/2}C_b\pi^{-1/2}t^{-1/2}$$

where  $D$  represents the diffusion coefficient ( $\text{cm}^2 \text{s}^{-1}$ ), and  $C_b$  is the applied bulk concentration ( $\text{mol cm}^{-3}$ ). Experimental results of  $I$  vs.  $t^{-1/2}$  were plotted in Figure 11A, with the best fits for different concentrations of BHA. The resulting slopes, corresponding to straight lines in Figure 11A, were then plotted against the concentration of BHA (Figure 11B). The mean value of  $D$  was determined to be  $8.2 \times 10^{-5} \text{ cm}^2/\text{s}$  according to the resulting slope and Cottrell equation.

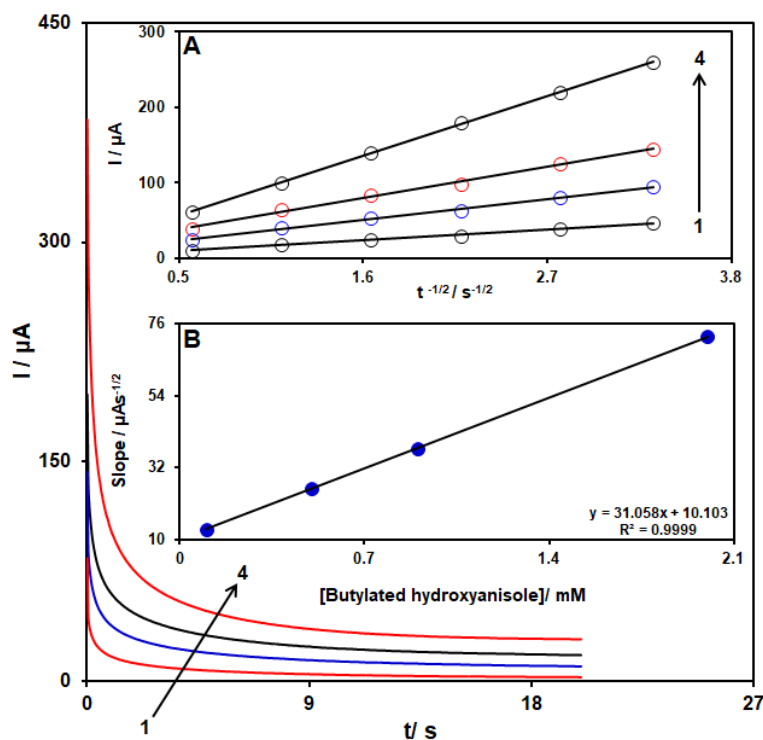


**Figure 11.** Chronoamperograms obtained at  $[\text{Co}(\text{HL})_2\text{Cl}_2]$  nano-complex/GCE in 0.1 M PBS (pH 7.0) for different concentration of BHA. The 1-4 correspond to 0.1, 0.5, 0.9, and 2.0 mM of BHA. Insets: (A) Plots of  $I$  vs.  $t^{-1/2}$  obtained from chronoamperograms 1-4. (B) Plot of the slope of the straight lines against BHA concentration.

### Calibration curve

Because DPV commonly has a higher sensitivity than CV, the DPV technique was applied for the quantitative detection of BHA. Figure 12 shows the differential pulse voltammograms of BHA at various concentrations using  $[\text{Co}(\text{HL})_2\text{Cl}_2]$  nano-complex/GCE. As seen, the oxidation peak currents of BHA enhance gradually by increasing its concentration. The oxidation peak currents ( $I_{pa}$ ) show a good linear relationship with the concentrations of BHA ranging from 0.5 M to 150.0  $\mu\text{M}$ . The linear equation is  $I_{pa}/\mu\text{A} = 0.171C_{\text{BHA}}/\mu\text{M} + 0.4624$  ( $R^2 = 0.9994$ ) (Figure 12 (inset)). Also, the limit of detection,  $C_m$ , of BHA was calculated using the following equation:

$$C_m = 3S_b/m$$

where,  $m$  is the slope of the calibration plot ( $0.171 \mu\text{A}/\mu\text{M}$ ) and  $S_b$  is the standard deviation of the blank response obtained from 15 replicate measurements of the blank solution. The detection limit for determination of BHA using this method of  $0.12 \mu\text{M}$  was obtained.

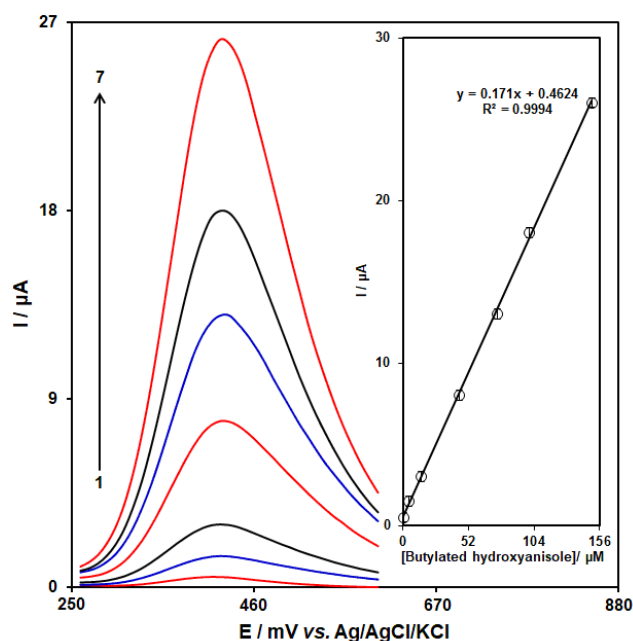


**Figure 12.** DPVs of  $[\text{Co}(\text{HL})_2\text{Cl}_2]$  nano-complex/GCE in 0.1 M (pH 7.0) containing different concentrations of BHA. Numbers 1–7 correspond to 0.5, 5.0, 15.0, 45.0, 75.0, 100.0, and 150.0  $\mu\text{M}$  of BHA. Inset: plot of the electrocatalytic peak current as a function of BHA concentration in the range of 0.5–150.0  $\mu\text{M}$ .

## Conclusions

We have reported the synthesis of a Schiff base ligand and a new Co(II) complex (**1**). The [HL] and its cobalt(II) complex (**1**) were characterized by spectroscopic techniques and elemental analysis. The single crystal X-ray diffraction analysis of the complex showed that metal ions reacted with the ligand in a 1:2 molar ratio. In the formation of the complex, oxygen atoms of two ligands are coordinated to the metal ion, and tetrahedral geometry is formed around the metal ion with two chloride ions attached to it. Also, the nanocomplex (**2**) have been synthesized by the sonochemical process. The nanocomplex (**2**) was characterized via X-ray powder diffraction (XRD) and SEM. The XRD patterns indicated both (**1**) and (**2**) compounds prepared by different synthesis methods have the same crystal structure. A sensitive and fast voltammetric method to detect the BHA based on  $[\text{Co}(\text{HL})_2\text{Cl}_2]$  nano-complex (**2**) modified glassy carbon electrode was established. The voltammetric investigation demonstrates that electrooxidation of BHA at the surface of  $[\text{Co}(\text{HL})_2\text{Cl}_2]$  nano-complex/GCE showed very distinct characteristics due to the presence of nanoparticles of  $[\text{Co}(\text{HL})_2\text{Cl}_2]$  complex on the surface of electrode.  $[\text{Co}(\text{HL})_2\text{Cl}_2]$  nano-complex/GCE exhibited good catalytic activity towards the oxidation of BHA over a linear range from 0.5 to 150.0  $\mu\text{M}$  with an enhanced sensitivity of 0.171  $\mu\text{A}/\mu\text{M}$  of BHA and favourable characteristics for the determination of BHA with a detection limit of 0.12  $\mu\text{M}$ . Finally, the proposed method was successfully applied in the determination of BHA in real samples with satisfactory results.

**Acknowledgment:** The authors sincerely thank the University of Sistan and Baluchestan for providing financial support for this work.

**Conflict of interest:** The authors declare no conflict of interest.

## References

- [1] K.H.G. Freitas, O. Fatibello-Filho. Simultaneous determination of butylated hydroxyanisole (BHA) and butylated hydroxytoluene (BHT) in food samples using a carbon composite electrode modified with  $\text{Cu}_3(\text{PO}_4)_2$  immobilized in polyester resin. *Talanta* **81** (2010) 1102–1108. <https://doi.org/10.1016/j.talanta.2010.02.004>
- [2] D. Thomas, Z. Rasheed, J.S. Jagan, K.G. Kumar. Study of kinetic parameters and development of a voltammetric sensor for the determination of butylated hydroxyanisole (BHA) in oil samples. *Journal of Food Science and Technology* **52** (2015) 6719–6726. <https://doi.org/10.1007/s13197-015-1796-1>

- [3] S.R. Prabakar, S.S. Narayanan. Surface modification of amine-functionalised graphite for preparation of cobalt hexacyanoferrate (CoHCF)-modified electrode: an amperometric sensor for determination of butylated hydroxyanisole (BHA). *Analytical and Bioanalytical Chemistry* **386** (2006) 2107-2115. <https://doi.org/10.1007/s00216-006-0854-y>
- [4] M. Cui, S. Liu, W. Lian, J. Li, W. Xu, J. Huang. A molecularly-imprinted electrochemical sensor based on a graphene–Prussian blue composite-modified glassy carbon electrode for the detection of butylated hydroxyanisole in foodstuffs. *Analyst* **138** (2013) 5949-5955. <https://doi.org/10.1039/C3AN01190A>
- [5] Z. Rasheed, A.E. Vikraman, D. Thomas, J.S. Jagan, K.G. Kumar. Carbon-nanotube-based sensor for the determination of butylated hydroxyanisole in food samples. *Food Analytical Methods* **8** (2015) 213-221. <https://doi.org/10.1007/s12161-014-9894-7>
- [6] L.F. Capitán-Vallvey, M.C. Valencia, E.A. Nicolás. Simple resolution of butylated hydroxyanisole and n-propyl gallate in fatty foods and cosmetics samples by flow-injection solid-phase spectrophotometry. *Journal of Food Science* **68(5)** (2003) 1595-1599. <https://doi.org/10.1111/j.1365-2621.2003.tb12297.x>
- [7] N.B. Tombesi, H. Freije, Application of solid-phase microextraction combined with gas chromatography–mass spectrometry to the determination of butylated hydroxytoluene in bottled drinking water. *Journal of Chromatography A* **963** (2002) 179-183. [https://doi.org/10.1016/S0021-9673\(02\)00217-0](https://doi.org/10.1016/S0021-9673(02)00217-0)
- [8] A. Sanches-Silva, J.M. Cruz, R. Sendón-García, P. Paseiro-Losada. Determination of butylated hydroxytoluene in food samples by high-performance liquid chromatography with ultraviolet detection and gas chromatography/mass spectrometry. *Journal of AOAC International* **90** (2007) 277-283. <https://doi.org/10.1093/jaoac/90.1.277>
- [9] Y. Guan, Q. Chu, L. Fu, T. Wu, J. Ye. Determination of phenolic antioxidants by micellar electrokinetic capillary chromatography with electrochemical detection. *Food Chemistry* **94** (2006) 157-162. <https://doi.org/10.1016/j.foodchem.2005.01.015>
- [10] S. Han, Y. Ding, F. Teng, A. Yao, Q. Leng. Molecularly imprinted electrochemical sensor based on 3D-flower-like MoS<sub>2</sub> decorated with silver nanoparticles for highly selective detection of butylated hydroxyanisole. *Food Chemistry* **387** (2022) 132899. <https://doi.org/10.1016/j.foodchem.2022.132899>
- [11] N.S. Sangeetha, S.S. Narayanan. Effective electrochemical detection of riboflavin and butylated hydroxy anisole based on azure A and nickel hexacyanoferrate framework on graphite electrode. *Chemical Data Collections* **30** (2020) 100544. <https://doi.org/10.1016/j.cdc.2020.100544>
- [12] H. Karimi-Maleh, R. Darabi, M. Shabani-Nooshabadi, M. Baghayeri, F. Karimi, J. Rouhi, C. Karaman. Determination of D&C Red 33 and Patent Blue V Azo dyes using an impressive electrochemical sensor based on carbon paste electrode modified with ZIF-8/g-C<sub>3</sub>N<sub>4</sub>/Co and ionic liquid in mouthwash and toothpaste as real samples. *Food and Chemical Toxicology* (2022) 112907. <https://doi.org/10.1016/j.fct.2022.112907>
- [13] H. Peyman, H. Roshanfekar, A. Babakhanian, H. Jafari. PVC Membrane Electrode Modified by Lawson as Synthetic Derivative Ionophore for Determination of Cadmium in Alloy and Wastewater. *Chemical Methodologie* **5(5)** (2020) 446-453. [http://www.chemmethod.com/article\\_135266.html](http://www.chemmethod.com/article_135266.html)
- [14] H. Beitollahi, S.Z. Mohammadi, M. Safaei, S. Tajik. Applications of electrochemical sensors and biosensors based on modified screen-printed electrodes: a review. *Analytical Methods* **12** (2020) 1547-1560. <https://doi.org/10.1039/C9AY02598G>
- [15] S. Saghiri, M. Ebrahimi, M.R. Bozorgmehr. NiO nanoparticle/1-hexyl-3-methylimidazolium hexafluorophosphate composite for amplification of epinephrine electrochemical sensor. *Asian Journal of Nanosciences and Materials* **4** (2021) 46-52. <https://doi.org/10.26655/AJNANOMAT.2021.1.4>
- [16] Y.F. Mustafa, G. Chehardoli, S. Habibzadeh, Z. Arzehgar. Electrochemical detection of sulfite in food samples. *Journal of Electrochemical Science and Engineering* **12** (2022) 1061-1079. <https://doi.org/10.5599/jese.1555>
- [17] T. Eren, N. Atar, M. L. Yola, H. Karimi-Maleh. A sensitive molecularly imprinted polymer based quartz crystal microbalance nanosensor for selective determination of lovastatin in red yeast rice. *Food Chemistry* **185** (2015) 430-436. <https://doi.org/10.1016/j.foodchem.2015.03.153>

- [18] M.S. Sengar, S. Saxena, S.P. Satsangee, R. Jain. Silver Nanoparticles Decorated Functionalized Multiwalled Carbon Nanotubes Modified Screen Printed Sensor for Voltammetric Determination of Butorphanol. *Journal of Applied Organometallic Chemistry* **1** (2021) 95-108. <https://doi.org/10.22034/jaoc.2021.289344.1023>
- [19] M. Mazloum-Ardakani, H. Beitollahi, B. Ganjipour, H. Naeimi. Novel carbon nanotube paste electrode for simultaneous determination of norepinephrine, uric acid and d-penicillamine. *International Journal of Electrochemical Science* **5** (2010) 531-546.
- [20] A. Lohrasbi-Nejad. Electrochemical strategies for detection of diazinon. *Journal of Electrochemical Science and Engineering* **12** (2022) 1041-1059. <https://doi.org/10.5599/jese.1379>
- [21] H. Karimi-Maleh, A.F. Shojaei, K. Tabatabaieian, F. Karimi, S. Shakeri, R. Moradi. Simultaneous determination of 6-mercaptopruine, 6-thioguanine and dasatinib as three important anticancer drugs using nanostructure voltammetric sensor employing Pt/MWCNTs and 1-butyl-3-methylimidazolium hexafluoro phosphate. *Biosensors and Bioelectronics* **86** (2016) 879-884. <https://doi.org/10.1016/j.bios.2016.07.086>
- [22] Z. Mehdizadeh, S. Shahidi, A. Ghorbani-HasanSaraei, M. Limooei, M. Bijad. Monitoring of Amaranth in Drinking Samples using Voltammetric Amplified Electroanalytical Sensor. *Chemical Methodologies* **6** (2022) 246-252. <https://doi.org/10.22034/chemm.2022.324073.1423>
- [23] S. Tajik, H. Beitollahi, F.G. Nejad, I.S. Shoaie, M.A. Khalilzadeh, M.S. Asl, M. Shokouhimehr. Recent developments in conducting polymers: Applications for electrochemistry. *RSC advances* **10(62)** (2020) 37834-37856. <https://doi.org/10.1039/D0RA06160C>
- [24] A. Shamsi, F. Ahour. Electrochemical Sensing of Thioridazine in Human Serum Samples Using Modified Glassy Carbon Electrode. *Advanced Journal of Chemistry-Section A* **4** (2021) 22-31. <https://doi.org/10.22034/ajca.2020.252025.1215>
- [25] P.M. Jahani. Flower-like MoS<sub>2</sub> screen-printed electrode based sensor for the sensitive detection of sunset yellow FCF in food samples. *Journal of Electrochemical Science and Engineering* **12** (2022) 1099-1109. <https://doi.org/10.5599/jese.1413>
- [26] S.A. Alavi-Tabari, M. A. Khalilzadeh, H. Karimi-Maleh. Simultaneous determination of doxorubicin and dasatinib as two breast anticancer drugs uses an amplified sensor with ionic liquid and ZnO nanoparticle. *Journal of Electroanalytical Chemistry* **811** (2018) 84-88. <https://doi.org/10.1016/j.jelechem.2018.01.034>
- [27] S. Azimi, M. Amiri, H. Imanzadeh, A. Bezaatpour. Fe<sub>3</sub>O<sub>4</sub>@SiO<sub>2</sub>-NH<sub>2</sub>/CoSB Modified Carbon Paste Electrode for Simultaneous Detection of Acetaminophen and Chlorpheniramine. *Advanced Journal of Chemistry-Section A* **4** (2021) 152-164. <https://doi.org/10.22034/ajca.2021.275901.1246>
- [28] S. Tajik, M.A. Taher, H. Beitollahi. First report for simultaneous determination of methyl dopa and hydrochlorothiazide using a nanostructured based electrochemical sensor. *Journal of Electroanalytical Chemistry* **704** (2013) 137-144. <https://doi.org/10.1016/j.jelechem.2013.07.008>
- [29] M. Vardini, N. Abbasi, A. Kaviani, M. Ahmadi, E. Karimi. Graphite Electrode Potentiometric Sensor Modified by Surface Imprinted Silica Gel to Measure Valproic Acid. *Chemical Methodologies* **6** (2022) 398-408. [http://www.chemmethod.com/article\\_147528.html](http://www.chemmethod.com/article_147528.html)
- [30] S. Ariavand, M. Ebrahimi, E. Foladi. Design and Construction of a Novel and an Efficient Potentiometric Sensor for Determination of Sodium Ion in Urban Water Samples. *Chemical Methodologies* **6(11)** (2022) 886-904. <https://doi.org/10.22034/chemm.2022.348712.1567>
- [31] H. Karimi-Maleh, M. Sheikhshoaie, I. Sheikhshoaie, M. Ranjbar, J. Alizadeh, N.W. Maxakato, A. Abbaspourrad. A novel electrochemical epinine sensor using amplified CuO nanoparticles and an-hexyl-3-methylimidazolium hexafluorophosphate electrode. *New Journal of Chemistry* **43** (2019), 2362-2367. <https://doi.org/10.1039/C8NJ05581E>
- [32] R.M. Mohabis, F. Fazeli, I. Amini, V. Azizkhani. An overview of recent advances in the detection of ascorbic acid by electrochemical techniques. *Journal of Electrochemical Science and Engineering* **12** (2022) 1081-1098. <https://doi.org/10.5599/jese.1561>

- [33] S. Tajik, M.A. Taher, H. Beitollahi. Simultaneous determination of droxidopa and carbidopa using a carbon nanotubes paste electrode. *Sensors and Actuators B: Chemical* **188** (2013) 923-930. <https://doi.org/10.1016/j.snb.2013.07.085>
- [34] A. Hosseini Fakhrrabad, R. Sanavi Khoshnood, M.R. Abedi, M. Ebrahimi. Fabrication a composite carbon paste electrodes (CPEs) modified with multi-wall carbon nano-tubes (MWCNTs/N, N-Bis (salicyliden)-1,3-propandiamine) for determination of lanthanum (III). *Eurasian Chemical Communications* **3** (2021) 627-634. <https://doi.org/10.22034/ecc.2021.288271.1182>
- [35] K. Harismah, M. Mirzaei, M. Dai, Z. Roshandel, E. Salarrezaei. In silico investigation of nanocarbon biosensors for diagnosis of COVID-19. *Eurasian Chemical Communications* **3(2)** (2021) 95-102. <https://doi.org/10.22034/ecc.2021.267226.1120>
- [36] H. Karimi-Maleh, C. Karaman, O. Karaman, F. Karimi, Y. Vasseghian, L. Fu, A. Mirabi. Nanochemistry approach for the fabrication of Fe and N co-decorated biomass-derived activated carbon frameworks: a promising oxygen reduction reaction electrocatalyst in neutral media. *Journal of Nanostructure in Chemistry* (2022) 1-11. <https://doi.org/10.1007/s40097-022-00492-3>
- [37] A. Dehno Khalaji, P. Machek, M. Jarosova,  $\alpha$ -Fe<sub>2</sub>O<sub>3</sub> Nanoparticles: Synthesis, Characterization, Magnetic Properties and Photocatalytic Degradation of Methyl Orange. *Advanced Journal of Chemistry-Section A* **4(4)** (2021) 317-326. <https://doi.org/10.22034/ajca.2021.292396.1268>
- [38] R. Hajinasir, M. Esmaeili Jadidi. Synthesis of ZnO nanoparticles via flaxseed aqueous extract. *Journal of Applied Organometallic Chemistry* **2(2)** (2022) 101-108. <https://doi.org/10.22034/jaoc.2022.154805>
- [39] M. Alidadykhoh, H. Pyman, H. Roshanfekar. Application of a New Polymer AgCl Nanoparticles Coated Polyethylene Terephthalat [PET] as Adsorbent for Removal and Electrochemical Determination of Methylene Blue Dye. *Chemical Methodologie* **5(2)** (2021) 96-106. <https://doi.org/10.22034/chemm.2021.119677>
- [40] N. Koozhadi, Z. Rezayati Zad. A Highly Sensitive Colorimetric Determination of Paraquat by Silver Nanoparticles. *Advanced Journal of Chemistry-Section B: Natural Products and Medical Chemistry* **3(4)** (2021) 311-322. <https://doi.org/10.22034/ajcb.2021.302596.1092>
- [41] M. Miraki, H. Karimi-Maleh, M.A. Taher, S. Cheraghi, F. Karimi, S. Agarwal, V.K. Gupta. Voltammetric amplified platform based on ionic liquid/NiO nanocomposite for determination of benserazide and levodopa. *Journal of Molecular Liquids* **278** (2019) 672-676. <https://doi.org/10.1016/j.molliq.2019.01.081>
- [42] H. Beitollahi, I. Sheikhshoae. Novel nanostructure-based electrochemical sensor for simultaneous determination of dopamine and acetaminophen. *Materials Science and Engineering: C* **32(2)** (2012) 375-380. <https://doi.org/10.1016/j.msec.2011.11.009>
- [43] M. Bijad, A. Hojjati-Najafabadi, H. Asari-Bami, S. Habibzadeh, I. Amini, F. Fazeli. An overview of modified sensors with focus on electrochemical sensing of sulfite in food samples. *Eurasian Chemical Communications* **3(2)** (2021) 116-138. <https://doi.org/10.22034/ecc.2021.268819.1122>
- [44] A. Sahraei, H. Kargar, M. Hakimi, M.N. Tahir. Distorted square-antiprism geometry of new zirconium (IV) Schiff base complexes: Synthesis, spectral characterization, crystal structure and investigation of biological properties. *Journal of Molecular Structure* **1149** (2017) 576-584. <https://doi.org/10.1016/j.molstruc.2017.08.022>
- [45] A. Trzesowska-Kruszynska. Copper complex of glycine Schiff base: In situ ligand synthesis, structure, spectral, and thermal properties. *Journal of Molecular Structure* **1017** (2012) 72-78. <https://doi.org/10.1016/j.molstruc.2012.03.003>
- [46] J. Joseph, G.A.B. Rani. Metal based SOD mimetic therapeutic agents: Synthesis, characterization and biochemical studies of metal complexes. *Arabian Journal of Chemistry* **10** (2017) S1963-S1972. <https://doi.org/10.1016/j.arabjc.2013.07.024>
- [47] X. Liu, J.R. Hamon. Recent developments in penta-, hexa-and heptadentate Schiff base ligands and their metal complexes. *Coordination Chemistry Reviews* **389** (2019) 94-118. <https://doi.org/10.1016/j.ccr.2019.03.010>

- [48] S. Kaya, S. Erkan, D. Karakaş. Computational investigation of molecular structures, spectroscopic properties and antitumor-antibacterial activities of some Schiff bases. *Spectrochimica Acta Part A: Molecular and Biomolecular Spectroscopy* **244** (2021) 118829. <https://doi.org/10.1016/j.saa.2020.118829>
- [49] A.M. Abu-Dief, I.M. Mohamed. A review on versatile applications of transition metal complexes incorporating Schiff bases. *Beni-suef University Journal of Basic and Applied Sciences* **4(2)** (2015) 119-133. <https://doi.org/10.1016/j.bjbas.2015.05.004>
- [50] S.A. Dailami, S.A. Onakpa, M.A. Funtua. Fe (III) and Cr (III) Complexes with Phenolic Schiff Base: Synthesis, Physico-Chemical Characterisation, Antimicrobial and Antioxidant Studies. *IOSR Journal of Applied Chemistry* **9(9)** (2016) 18-23.
- [51] E. Tozzo, S. Romera, M.P. dos Santos, M. Muraro, H.D.A. Regina, L.M. Liao, E.R. Dockal. Synthesis, spectral studies and X-ray crystal structure of N, N'-(±)-trans-1, 2-cyclohexylenebis (3-ethoxysalicylideneamine) H<sub>2</sub> (t-3-EtOsalchxn). *Journal of Molecular Structure* **876** (2008) 110-120. <https://doi.org/10.1016/j.molstruc.2007.05.043>
- [52] M. Masoudi, M. Behzad, A. Arab, A. Tarahhomi, H.A. Rudbari, G. Bruno. Crystal structures, DFT calculations and Hirshfeld surface analyses of three new cobalt (III) Schiff base complexes derived from meso-1, 2-diphenyl-1, 2-ethylenediamine. *Journal of Molecular Structure* **1122** (2016) 123-133. <https://doi.org/10.1016/j.molstruc.2016.05.092>
- [53] P.G. Cozzi. Metal–Salen Schiff base complexes in catalysis: practical aspects. *Chemical Society Reviews* **33** (2004) 410-421. <https://doi.org/10.1039/B307853C>
- [54] O. Fatibello-Filho, E.R. Dockal, L.H. Marcolino-Junior, M.F. Teixeira. Electrochemical modified electrodes based on metal-salen complexes. *Analytical letters* **40** (2007) 1825-1852. <https://doi.org/10.1080/00032710701487122>
- [55] W. Al Zoubi, N. Al Mohanna. Membrane sensors based on Schiff bases as chelating ionophores—A review. *Spectrochimica Acta Part A: Molecular and Biomolecular Spectroscopy* **132** (2014) 854-870. <https://doi.org/10.1016/j.saa.2014.04.176>
- [56] É.N. Oiyé, M.F.M. Ribeiro, J.M.T. Katayama, M.C. Tadini, M.A. Balbino, I.C. Eleotério, M.F. de Oliveira. Electrochemical sensors containing Schiff bases and their transition metal complexes to detect analytes of forensic, pharmaceutical and environmental interest. A review. *Critical Reviews in Analytical Chemistry* **49(6)** (2019) 488-509. <https://doi.org/10.1080/10408347.2018.1561242>
- [57] R.H. Taha, Z.A. El-Shafiey, A.A. Salman, E.M. El-Fakharany, M.M. Mansour. Synthesis and characterization of newly synthesized Schiff base ligand and its metal complexes as potent anticancer. *Journal of Molecular Structure* **1181** (2019) 536-545. <https://doi.org/10.1016/j.molstruc.2018.12.055>
- [58] E. Yousif, A. Majeed, K. Al-Sammarae, N. Salih, J. Salimon, B. Abdullah. Metal complexes of Schiff base: preparation, characterization and antibacterial activity. *Arabian Journal of Chemistry* **10** (2017) S1639-S1644. <https://doi.org/10.1016/j.arabjc.2013.06.006>
- [59] M. Biabani, H. Saravani, V. Eigner, M. Dusek. A novel coordination polymer of Cd (II) based on 2-mercaptopyrimidine: sonochemical synthesis, characterization, and antibacterial properties. *Journal of Molecular Structure* **1166** (2018) 470-478. <https://doi.org/10.1016/j.molstruc.2018.04.054>
- [60] H. Sadeghzadeh, A. Morsali. Sonochemical synthesis and characterization of nano-belt lead (II) coordination polymer: new precursor to produce pure phase nano-sized lead (II) oxide. *Ultrasonics Sonochemistry* **18(1)** (2011) 80-84. <https://doi.org/10.1016/j.ultsonch.2010.01.011>
- [61] M. Saif, H.F. El-Shafiy, M.M. Mashaly, M.F. Eid, A.I. Nabeel, R. Fouad. Synthesis, characterization, and antioxidant/cytotoxic activity of new chromone Schiff base nano-complexes of Zn (II), Cu (II), Ni (II) and Co (II). *Journal of Molecular Structure* **1118** (2016) 75-82. <https://doi.org/10.1016/j.molstruc.2016.03.060>

